ELSEVIER

Polymer 42 (2001) 3183–3194

polymer

www.elsevier.nl/locate/polymer

Photophysical characterization of diphenyl-substituted phenylenevinylene and diphenylenevinylene polymers

W. Holzer[a], A. Penzkofer[a,*], R. Stockmann[b], H. Meysel[b], H. Liebegott[b], H.H. Hörhold[b]

[a]*Institut II — Experimentelle und Angewandte Physik, Universität Regensburg, Universitätsstraße 31, D-93040 Regensburg, Germany*
[b]*INNOVENT Technologieentwicklung e.V., D-07745 Jena, und Institut für Organische Chemie und Makromolekulare Chemie der Universität Jena, Humboldtstrasse 10, D-07743 Jena, Germany*

Received 7 April 2000; accepted 5 July 2000

Abstract

Neat films and solutions of poly[1,4-phenylene-1,2-di(4-phenoxyphenyl)vinylene], poly[1,4-phenylene-1,2-di(phenthiophenyl)vinylene], poly[4,4′-diphenylene-1,2-di(4-phenoxyphenyl)vinylene] and poly[4,4′-diphenylene-1,2-di(4-fluorophenyl)vinylene] in 1,4-dioxane are investigated. The optical constants of the neat films are determined, absorption and fluorescence data are analysed, and picosecond laser saturable absorption studies are carried out. The fluorescence lifetimes and fluorescence quantum yields are analysed to determine the emitting chromophore size (electronic delocalization). The saturable absorption measurements are used to determine the average absorption segment size.

Keywords: Luminescent polymers; Phenylenevinylene polymers; Diphenylenevinylene polymers

1. Introduction

Diphenyl substituted phenylenevinylene polymers found strong interest as nonlinear optical materials in opto-optical waveguide switching elements [1–5]. They are used as electro-luminescent layers in organic light-emitting diodes (OLEDs) [6–8]. Most studies have been carried out on poly[1,4-phenylene-1,2-diphenoxyphenylvinylene] (DPOP-PPV). The third-order nonlinear optical properties (nonlinear refractive index n_2 [1,3,9], two-photon absorption coefficient β [1,3,9] and third-order nonlinear susceptibility $\chi^{(3)}$ [5]) have been determined. The absorption [1,10], photoluminescence [6,10], electroluminescence [6] and photoconductivity [7,11,12] have been studied. Picosecond time-resolved pump and probe laser experiments revealed photoinduced absorption spectra [13]. The carrier transport in LED structures was determined by time-of-flight measurements [7]. Conformation studies were performed by X-ray diffraction [14]. Photoelectron spectroscopic studies and semi-empirical chemical calculations have been carried out for poly(4,4-diphenylene diphenylvinylene) [15]. The phenyl substitution at the vinylene carbon position of the phenylenevinylene polymers reduces the tendency of oxidation [8].

Here we investigate the two diphenyl-substituted phenylenevinylene polymers DPOP-PPV and poly[1,4-phenylene-1,2-di(phenthiophenyl)vinylene] DPSP-PPV as well as the two diphenyl-substituted diphenylenevinylene polymers poly[4,4′-diphenylene-1,2-di(4-phenoxyphenyl)-vinylene] DPOP-PDPV and poly[4,4′-diphenylene-1,2-di(4-fluorophenyl)vinylene] DFP-PDPV. Their structural formulae, full names, molar masses, degrees of polymerization and glass transition temperatures are given in Fig. 1. Neat films and 1,4-dioxane solutions are studied. The optical constants of the neat films are determined. Absorption and fluorescence spectra are measured and analysed. Picosecond laser saturable absorption studies are carried out. The fluorescence lifetimes and fluorescence quantum yields are analysed to determine the chromophore size of light emission (exciton size, excitation delocalization). The saturable absorption data are compared with numerical simulations to determine the average segment size that takes part in conformational relaxation after single-photon excitation.

2. Experimental

The synthesis of the polymers is described in Refs. [16–20]. They were prepared by reductive coupling

* Corresponding author. Tel.: +49-941-943-2107; fax: +49-941-9432754.
E-mail address: alfons.penzkofer@physik.uni-regensburg.de (A. Penzkofer).

0032-3861/01/$ - see front matter
PII: S0032-3861(00)00522-X

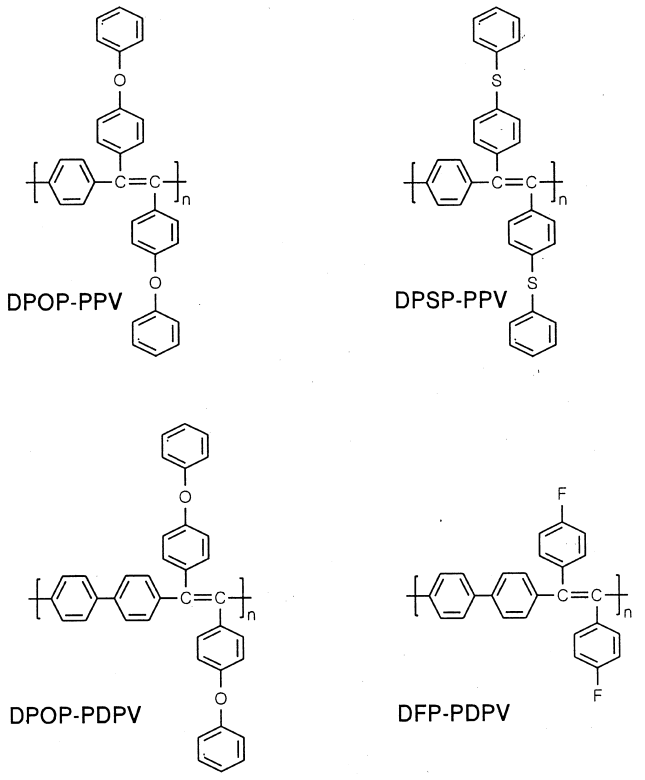

Fig. 1. Structural formula of repeat units of the investigated polymers. DPOP-PPV: $C_{32}H_{22}O_2$. Molar mass of repeat unit. $M = 438.53$ g mol^{-1}. Number-average molar mass $M_n = 16\,400$ g mol^{-1}. Weight-average molar mass $M_w = 23\,800$ g mol^{-1}. M_n and M_w are determined by gel permeation chromatography using polystyrene standards. Degree of polymerization $DP_w = M_w/M = 54.3$. Polydispersivity $M_w/M_n = 1.42$. Glass transition temperature, $T_g = 161$°C (from differential scanning calorimetry). DPSP-PPV: $C_{32}H_{22}S_2$. $M = 470.66$ g mol^{-1}. $M_n = 20\,300$ g mol^{-1}. $M_w = 45\,400$ g mol^{-1}. $DP_w = 96.4$. $M_w/M_n = 2.24$. $T_g = 137$°C. DPOP-PDPV: $C_{38}H_{26}O_2$. $M = 514.62$ g mol^{-1}. $M_n = 13\,700$ g mol^{-1}. $M_w = 20\,400$ g mol^{-1}. $DP_w = 39.6$. $M_w/M_n = 1.49$. $T_g = 183$°C. DFP-PDPV: $C_{26}H_{16}F_2$. $M = 366.41$ g mol^{-1}. $M_n = 39\,400$ g mol^{-1}. $M_w = 64\,800$ g mol^{-1}. $DP_w = 176.8$ $M_w/M_n = 1.64$. $T_g = 310$°C.

(dehalogenation polymerization) of appropriately substituted xylylene tetrachlorides. Neat films were prepared by dissolving the polymer powder in toluene (20 mg ml^{-1}) and spin-coating them on fused silica substrates. For liquid solution studies the polymers were dissolved in 1,4-dioxane.

The optical constants (refractive index spectrum, $n(\lambda)$ and absorption coefficient spectrum, $\alpha(\lambda)$) of the neat films were determined by reflectance and transmittance measurements [21,22]. The repeat-unit-based absorption cross-section spectra, $\sigma_a(\lambda)$, of 1,4-dioxane solutions are obtained by spectrophotometer transmission measurements. The neat-film absorption cross-section spectra are calibrated to the solution spectra (same absorption cross-section integrals) [23]. The fluorescence quantum distributions, $E_F(\lambda)$, and the degrees of fluorescence polarization, $P_F(\lambda)$, are measured with a self-assembled fluorimeter [24]. The fluorescence data analysis (fluorescence quantum yield ϕ_F, radiative lifetime τ_{rad}, stimulated emission cross-section $\sigma_{em}(\lambda)$) is described in Ref. [23].

The fluorescence lifetimes are measured by picosecond pulse excitation (second harmonic pulses of an active and passive mode-locked ruby laser [25], pulse duration $\Delta t_L = 35$ ps, wavelength $\lambda_L = 347.15$ nm) and fast signal detection (Hamamatsu type R1564U-01 micro-channel plate photomultiplier and LeCroy type 9362 digital oscilloscope). The saturable absorption behaviour of the polymers in liquid solution is studied by transmission measurement of intense second-harmonic picosecond ruby laser pulses through the samples.

Relating the fluorescence lifetimes to the fluorescence quantum yields will be used to determine the emitting chromophore size [26,27]. The saturable absorption analysis will be used to get information on the absorption dynamics of the polymer segments [27–29].

3. Results

Transmittance and reflectance spectra of the investigated neat polymer films on fused silica substrates are shown in Fig. 2. The film thickness derived from the data analysis [21,22] is given in the figure caption. The extracted refractive index spectra, $n(\lambda)$, and absorption coefficient spectra, $\alpha(\lambda)$, [21,22] are displayed in Fig. 3. The absorption spectra have their maxima (S_0–S_1 absorption) around 370 nm. The refractive indices are largest around 400 nm. In the displayed wavelength region the neat film refractive indices

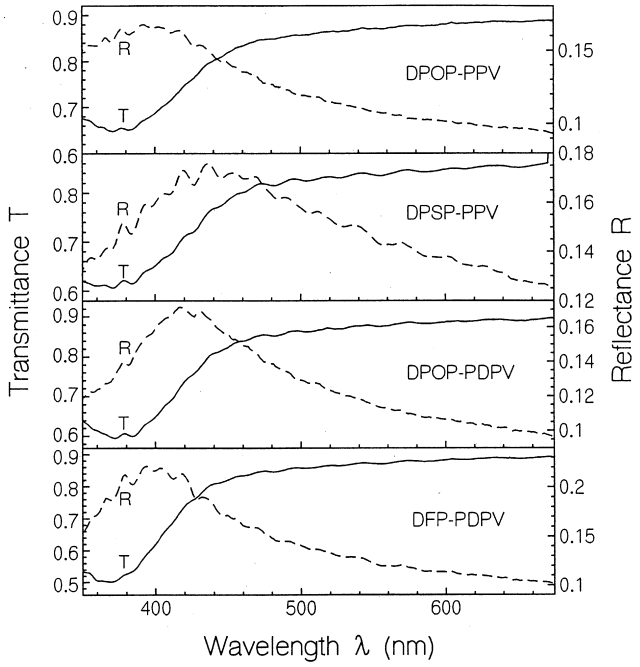

Fig. 2. Transmittance and reflectance spectra of neat films on fused silica substrates. Angle of incidence $\alpha = 12°$, s-polarized. (a) DPOP-PPV: film thickness, $d_f = 45$ nm. (b) DPSP-PPV: $d_f = 60$ nm. (c) DPOP-PDPV: $d_f = 45$ nm. (d) DFP-PDPV: $d_f = 40$ nm.

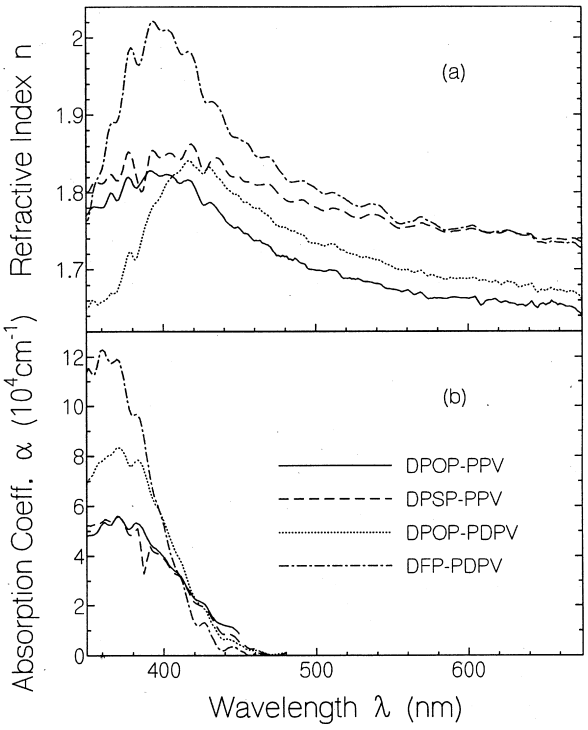

Fig. 3. (a) Refractive index spectra and (b) absorption coefficient spectra of neat thin films of DPOP-PPV (solid curves), DPSP-PPV (dashed curves), DPOP-PDPV (dotted curves) and DFP-PDPV (dash-dotted curves).

are well above the refractive index values of fused silica and of crown glasses. Therefore, waveguiding is possible in the neat polymer films on fused silica and crown glass substrates, if a minimum film thickness is surpassed [30].

The repeat-unit-based absorption cross-section spectra, $\sigma_a(\lambda)$, of the polymers in 1,4-dioxane (dotted curves) and of the neat polymer films (solid curves) are displayed in Fig. 4. The neat film spectra are quite similar to the solution spectra. Only some smoothing-out and long-wavelength extension of the absorption wings due to interchain interaction (enhancement of inhomogeneous broadening) is observed. The S_0–S_1-absorption peaks of the diphenylenevinylene polymers DPOP-PDPV and DFP-PDPV are roughly a factor of two larger than the S_0–S_1-absorption peaks of the phenylenevinylene polymers DPOP-PPV and DPSP-PPV.

The fluorescence quantum distributions, $E_F(\lambda)$, and the degrees of fluorescence polarization, $P_F(\lambda)$, of DPOP-PPV, DPSP-PPV, DPOP-PDPV and DFP-PDPV are displayed in Figs. 5–8, respectively. For each neat film fluorescence spectra, $E_F(\lambda)$, and polarization spectra, $P_F(\lambda)$, were measured for four different excitation wavelengths, λ_{exc} (312 nm, 365 nm, 405 nm, and 429 nm). The magnitudes and spectral shapes of the fluorescence quantum distributions are independent of the excitation wavelength. Only $E_F(\lambda)$ for $\lambda_{exc} = 365$ nm is shown in Figs. 5a, 6a, 7a and 8a. Within the fluorescence band the fluorescence polarization, $P_F(\lambda)$, decreases with rising wavelength, λ. The degree of fluorescence polarization increases with rising excitation wavelength, λ_{exc}. For $\lambda_{exc} = 312$ nm $P_F(\lambda)$ is approximately zero over the whole fluorescence region.

The triple-dashed curves in Figs. 5–8 show the $E_F(\lambda)$ and $P_F(\lambda)$ results for the polymers in 1,4-dioxane. The excitation wavelength was $\lambda_{exc} = 365$ nm. The shapes and wavelength positions of the fluorescence spectra, $E_F(\lambda)$, of the solutions are quite similar to the shapes and wavelength positions of fluorescence spectra of the neat films. Only the absolute values are reduced by approximately a factor of 10. The degree of fluorescence polarization of the solutions is higher than that of the neat films.

The Stokes shift, $\delta\tilde{\nu}_{abs,em}$, between the S_0–S_1 absorption peak and the S_1–S_0 emission peak are listed in Table 1. The shifts are rather large (absorption in the near UV, emission in the green-yellow region).

In Fig. 9 the fluorescence quantum yield, $\phi_F = \int E_F(\lambda)\, d\lambda$, and the degrees of fluorescence polarization, $P_F(\lambda = 550$ nm), versus excitation wavelength, λ_{exc}, are displayed for the neat films. The fluorescence quantum yield is wavelength independent within the accuracy of our measurement. The accuracy of fluorescence quantum yield measurement of highly fluorescent waveguiding neat films is influenced by the fluorescence absorption and reemission [27]. The inaccurate knowledge of the weak absorption in the fluorescence region limits the accuracy

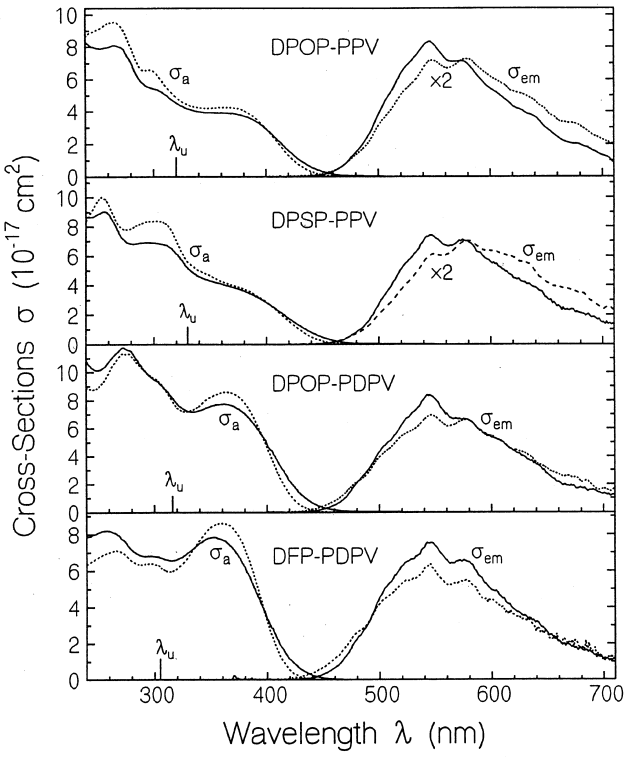

Fig. 4. Absorption cross-section spectra, σ_a, and stimulated emission cross-section spectra, σ_{em}, of neat films (solid curves) and 1,4-dioxane solutions (dotted curves) of DPOP-PPV, DPSP-PPV, DPOP-PDPV and DFP-PDPV.

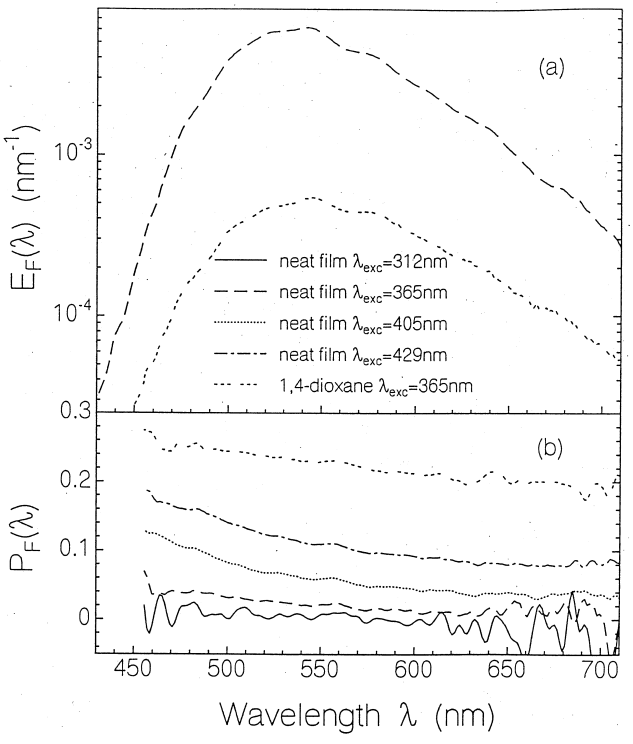

Fig. 5. (a) Fluorescence quantum distributions, $E_F(\lambda)$ and (b) degrees of fluorescence polarization, $P_F(\lambda)$, of DPOP-PPV neat films (thickness $d_f = 400$ nm) and DPOP-PPV in 1,4-dioxane (concentration $C = 1.2 \times 10^{-4}$ mol dm^{-3}). For the neat films the excitation wavelength, λ_{exc}, is varied.

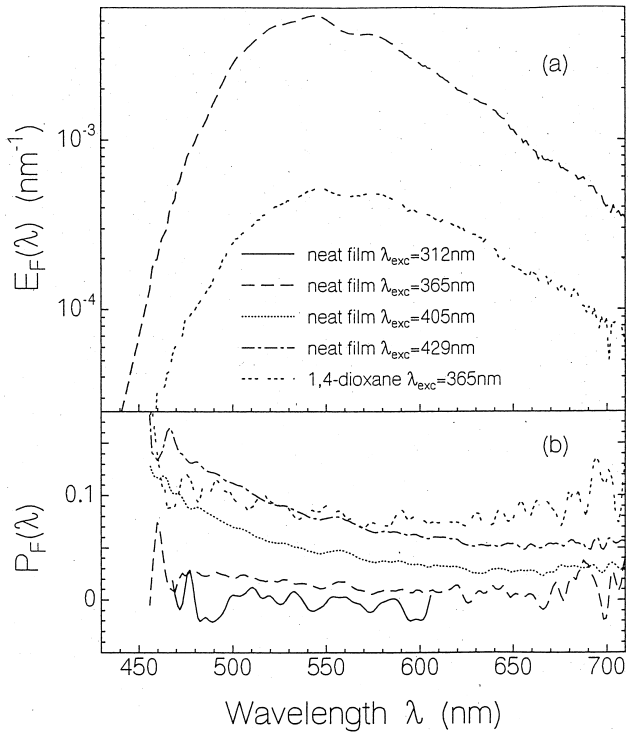

Fig. 6. (a) Fluorescence quantum distributions, $E_F(\lambda)$ and (b) degrees of fluorescence polarization, $P_F(\lambda)$, of DPSP-PPV neat films ($d_f = 510$ nm) and 1,4-dioxane solutions ($C = 7.1 \times 10^{-5}$ mol dm^{-3}). Excitation wavelength, λ_{exc}, is varied for the neat films.

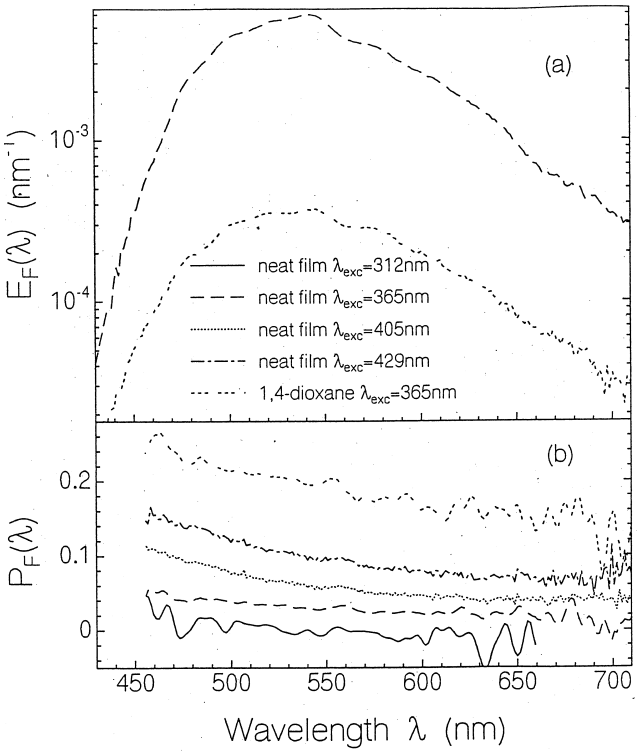

Fig. 7. (a) Fluorescence quantum distributions, $E_F(\lambda)$ and (b) degrees of fluorescence polarization, $P_F(\lambda)$, of DPOP-PDPV neat films ($d_f = 500$ nm) and 1,4-dioxane solutions ($C = 4.3 \times 10^{-5}$ mol dm^{-3}). Excitation wavelength is varied for the neat films.

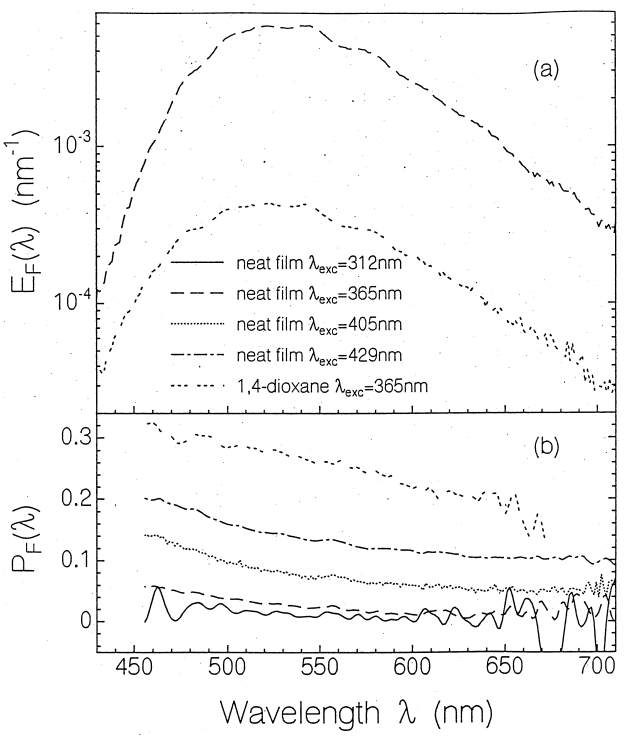

Fig. 8. (a) Fluorescence quantum distributions, $E_F(\lambda)$ and (b) degrees of fluorescence polarization, $P_F(\lambda)$, of DFP-PDPV neat films ($d_f = 510$ nm) and 1,4-dioxane solutions ($C = 6.0 \times 10^{-5}$ mol dm^{-3}). Excitation wavelength is varied for the neat films.

of ϕ_F determination to a few percent. The degree of fluorescence polarization, $P_F(\lambda = 550\ \text{nm})$, rises with excitation wavelength from nearly zero at $\lambda_{exc} = 312$ nm to about 10% at $\lambda_{exc} = 429$ nm.

The fluorescence quantum yields of the polymers in solution are listed in Table 1 (excitation wavelength 365 nm). They are in the 5–7% region. The degrees of fluorescence polarization at $\lambda = 550$ nm are also listed in Table 1 for the polymer solutions. With the exception of DPSP-PPV ($P_F \approx 0.083$) the degrees of fluorescence polarization are around 20%.

Temporal fluorescence signals of picosecond-pulse excited samples are shown in Fig. 10 (laser wavelength $\lambda_L = 347.15$ nm, pulse duration $\Delta t_L = 35$ ps). The dotted curves give the detector-oscilloscope response by directing attenuated picosecond excitation pulses directly to the detector. The solid curves belong to neat films and the dashed curves belong to 1,4-dioxane solutions. The fluorescence lifetimes, τ_F, (1/*e* signal decay times) extracted from the fluorescence signal decay curves are listed in Table 1. The fluorescence decay times of the neat films are around 1.5 ns, while fluorescence decay times of the solutions are in the 200–400 ps region.

The intensity dependent energy transmissions, $T_E(I_{0L})$ of intense picosecond pulses ($\lambda_L = 347.15$ nm, $\Delta t_L = 35$ ps) through samples of the polymers in 1,4-dioxane are displayed as circles in Figs. 11–13. For DPOP-PPV and DPSP-PPV the transmission practically does not change with excitation intensity (no absorption bleaching). For DPOP-PDPV (Fig. 12) and for DFP-PDPV (Fig. 13) a slight rise of transmission is observed with increasing excitation intensity.

4. Discussion

The linear absorption, nonlinear absorption and fluorescence data are analysed to extract parameters and to discuss the neat film and the solution behaviour of the polymers.

4.1. Linear absorption analysis

The repeat-unit-based S_0–S_1 absorption cross-section integrals, $\int_{S_0-S_1} \sigma_a(\tilde{\nu})\, d\tilde{\nu}$, are listed in Table 1. The upper borders of the S_0–S_1 absorption bands, $\lambda_u = \tilde{\nu}_u^{-1}$, are indicated in Fig. 4. The absorption cross-section integrals of the diphenyl-substituted diphenylenevinylene polymers DPOP-PDPV and DFP-PDPV are approximately a factor of 2 larger than the absorption cross-section integrals of the diphenyl-substituted phenylenevinylene polymers DPOP-PPV and DPSP-PPV.

The model compound tetraphenylethylene ($(C_6H_5)_2C{=}C(C_6H_5)_2$) has a similar absorption cross-section spectrum as DPOP-PDPV [31,32]. The spectrum is shown in Fig. 14. The S_0–S_1 absorption peak is only shifted about 50 nm to shorter wavelengths. The S_0–S_1 absorption cross-section integral of tetraphenylethylene is $\int_{S_0-S_1} \sigma_a(\tilde{\nu})\, d\tilde{\nu} \approx 3.47 \times 10^{-13}$ cm ($\lambda_u = 270$ nm). In Ref. [16] it is shown that for diphenyl-substituted phenylenevinylene oligomers the conjugation dependent absorption redshift reaches its limiting value already for a degree of polymerization of three. This finding indicates a limitation of an excitation interaction (vibronic coupling [33–35]) in these oligomers to about three repeat units.

4.2. Fluorescence analysis

The repeat-unit-based S_1-state radiative lifetimes, $\tau_{rad,RU}$, are calculated from the S_0–S_1 absorption cross-section spectra, $\sigma_a(\lambda)$, and the fluorescence quantum distributions, $E_F(\lambda)$, ($\lambda_{exc} = 365$ nm) by use of the Strickler–Berg formula [36–38]

$$\frac{1}{\tau_{rad,RU}} = \frac{8\pi c_0 n_F^3}{n_A} \frac{\int_{em} E_F(\lambda)\, d\lambda}{\int_{em} E_F(\lambda)\lambda^3\, d\lambda} \int_{abs} \frac{\sigma_a(\lambda)}{\lambda}\, d\lambda, \qquad (1)$$

where n_F and n_A are the average refractive indices in the fluorescence and absorption region, respectively, and c_0 is the speed of light in vacuum. The integrals extend over the S_1–S_0 emission wavelength region (em) and over the S_0–S_1 absorption band (abs). The resulting $\tau_{rad,RU}$ values are listed

Table 1
Spectroscopic parameters of the investigated polymers at room temperature

	DPVP-PPV		DPSP-PPV		DPOP-PDPV		DFP-PDPV	
	Solution	Neat film	Solution	Neat film	Solution	Neat film	Solution	Neat film
C (mol dm^{-3})	1.2×10^{-4}		7.1×10^{-5}		4.3×10^{-5}		6×10^{-5}	
$\tau_{rad,RU}$ (ns)	12.17	8.67	13.7	8.83	6.1	4.0	5.8	3.9
τ_F (ns)	0.46 ± 0.1	1.44 ± 0.12	0.44 ± 0.1	1.73 ± 0.12	0.31 ± 0.08	1.64 ± 0.07	0.25 ± 0.08	1.48 ± 0.2
ϕ_F[a]	0.073	0.72 ± 0.02	0.072	0.67 ± 0.02	0.051	0.705 ± 0.02	0.061	0.69 ± 0.02
τ_{rad} (ns)	6.3	2.1	6.1	2.5	6.1	2.3	4.1	2.1
m_e	1.93	4.1	2.25	3.5	1	1.8	1.4	1.9
P_F	0.23[b]	0.0214[a]	0.083[a]	0.0137[a]	0.196[a]	0.0285[a]	0.260[a]	0.024[a]
$\sigma_{a,L}$ (cm^2)	4.2×10^{-17}	3.95×10^{-17}	4.75×10^{-17}	4.4×10^{-17}	8.1×10^{-17}	7.5×10^{-17}	8.2×10^{-17}	7.75×10^{-17}
τ_{or} (ps)	325	54	73	41	150	83	200	62
$\int_{S_0-S_1}\sigma_a(\tilde{\nu})\,d\tilde{\nu}$ (cm)	2.96×10^{-13}	2.96×10^{-13}	2.67×10^{-13}	2.67×10^{-13}	5.47×10^{-13}	5.47×10^{-13}	5.58×10^{-13}	5.58×10^{-13}
$\delta\tilde{\nu}_{abs,em}$ (cm^{-1})	8700	8300	8800	8700	8800	8500	8900	9500
$I_{sat,s,RU}$ (W cm^{-2})	3.9×10^8	4.1×10^8	3.4×10^8	3.7×10^8	2.0×10^8	2.2×10^8	2.0×10^8	2.1×10^8
τ_{con}[c] (ps)	0.5	0.5	0.5	0.5	0.5	0.5	0.5	0.5
$\tau_{ex,L}$[d] (fs)	60	60	60	60	60	60	60	60
$\sigma_{ex,L}$ (cm^2)	$\approx 3.9\times10^{-17}$		$\approx 4.5\times10^{-17}$		$\approx 7.2\times10^{-17}$		$\approx 6\times10^{-17}$	
m_{seg}					6 ± 4		3 ± 1	

[a] $\lambda_{exc} = 365$ nm.
[b] $\lambda_{exc} = 405$ nm.
[c] Assumed [52]
[d] Assumed [53].

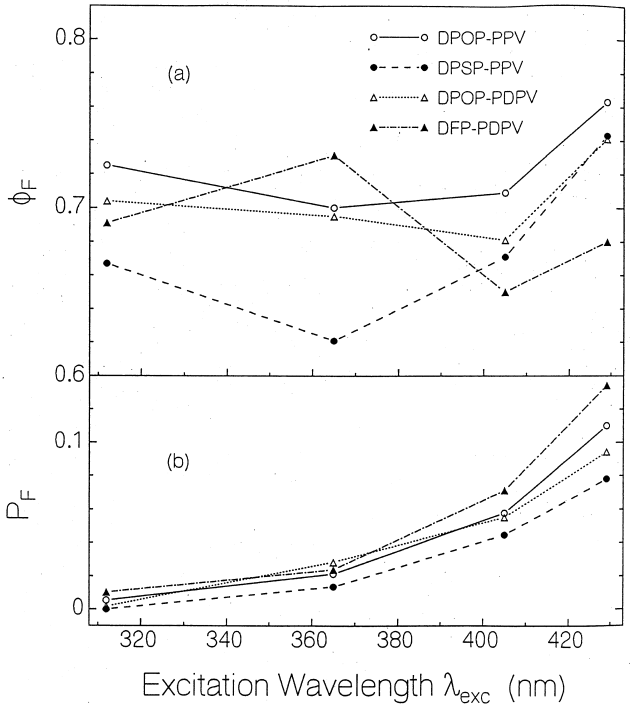

Fig. 9. (a) Fluorescence quantum yields, ϕ_F and (b) degrees of fluorescence polarization, P_F(550 nm), of neat films versus excitation wavelength. Measurements were carried out at marker positions.

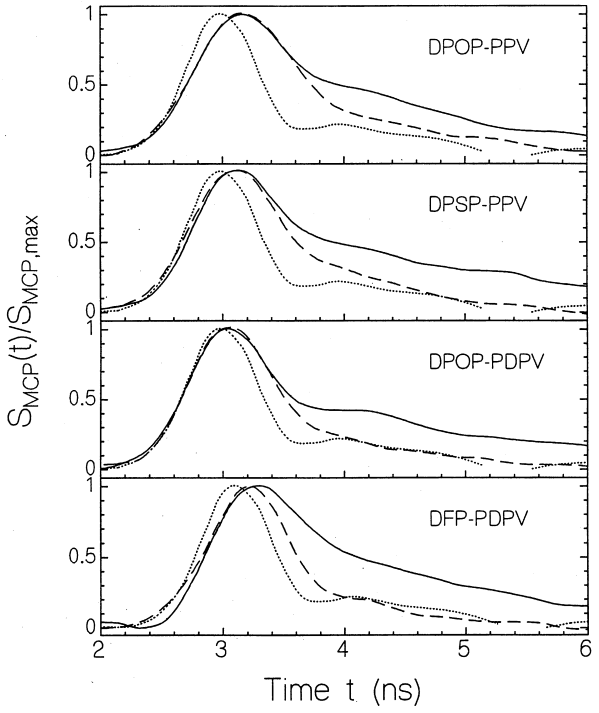

Fig. 10. Normalized temporal fluorescence signal heights, $S_{MCP}(t)/S_{MCP,max}$. Dotted curves, temporal response functions of micro-channelplate detector and fast digital oscilloscope (response to picosecond laser exposure). Solid curves, fluorescence signals of neat films. Dashed curves, fluorescence signal of 1,4-dioxane solutions.

in Table 1. The radiative lifetimes of the polymers in solution are longer than in neat films because of the smaller refractive index of 1,4-dioxane ($n = 1.4224$ at $\lambda =$ 589 nm [39]) compared to the neat films (see Fig. 3a).

The repeat-unit-based S_1–S_0 stimulated emission cross-section spectra, $\sigma_{em}(\lambda)$, are derived from the repeat-unit-based radiative lifetimes, $\tau_{rad,RU}$, and the fluorescence quantum distributions by use of the Einstein relation between absorption and emission [40,41]:

$$\sigma_{em}(\lambda) = \frac{\lambda^4 E_F(\lambda)}{8\pi c_0 n_F^2 \phi_F \tau_{rad,RU}}. \quad (2)$$

The calculated $\sigma_{em}(\lambda)$ spectra are displayed in Fig. 4. The spectra are similar for the 1,4-dioxane solutions and the neat films. Knowledge of the stimulated emission cross-section is important in laser material characterization.

The reorientation time, τ_{or}, of the S_0–S_1 transition dipole moments responsible for S_0–S_1 absorption and emission may be calculated from the degree of fluorescence polarization, P_F, (P_F at $\lambda = 550$ nm is used here) and the fluorescence lifetime, τ_F, by use of the Perrin formula [42–44]:

$$\tau_{or} = \frac{1/P_0 - 1/3}{1 - P_F/P_0} P_F \tau_F \quad (3)$$

with $P_0 = 0.5$. The obtained data are listed in Table 1. The reorientation times of the polymers diluted in 1,4-dioxane are in the 100–300 ps range. The fast reorientation of the transition dipole moments seems to be due to intramolecular energy transfer in the coiled polymer chains. The reorientation times in the neat films are in the 40–80 ps range. The shortening of the reorientation time in neat films seems to be caused by additional inter-chain energy transfer.

The degree of fluorescence polarization, $P_F(\lambda)$, increases with rising excitation wavelength, λ_{exc} (Figs. 5b–8b and 9b). Within the fluorescence band $P_F(\lambda)$ reduces slightly with increasing emission wavelength, λ. An inhomogeneous distribution of the absorption band and the emission band seem to be responsible for this behaviour. The excess energy present in the case of short wavelength excitation allows an overcome of barriers and a relaxation to differently oriented segments of lower absorption and emission frequency. In the case of excitation at 312 nm the degree of fluorescence polarization is around zero. At this excitation wavelength S_0–S_2 excitation contributes to the absorption already. The S_0–S_2 transition dipole moments seem not to be oriented parallel to the S_0–S_1 transition dipole moments and therefore they reduce the degree of fluorescence polarization.

The fluorescence quantum yields of the polymers in 1,4-dioxane are approximately a factor of 10 lower than the fluorescence quantum in the stiff neat films. Both the vibrational, librational and rotational freedoms of motion of the side-chain substituents and the distortions of the main chain units seem to be responsible for fast nonradiative relaxation and reduced fluorescence quantum yield.

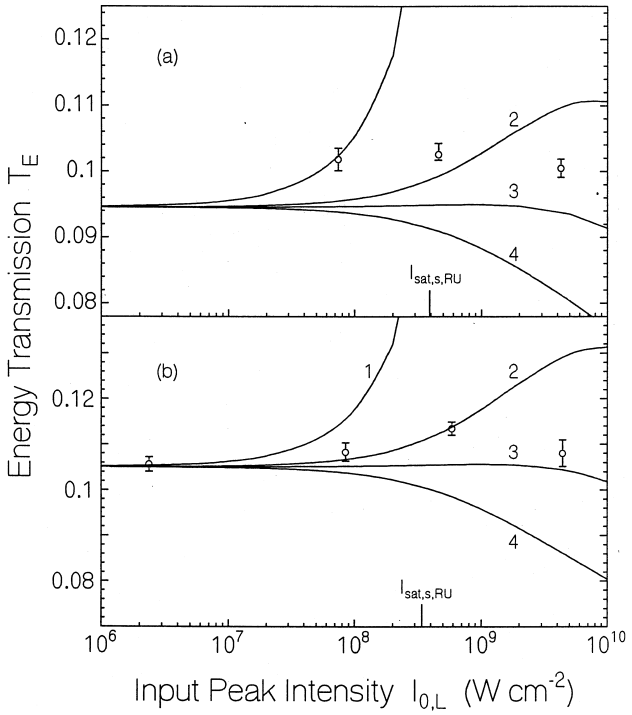

Fig. 11. Intensity-dependent energy transmission through DPOP-PPV and DPSP-PPV in 1,4-dioxane. Sample length, $l = 1$ mm. Circles are experimental points. The curves are calculated using parameters of Table 1 and $m_{seg} = 1$. (a) DPOP-PPV in 1,4-dioxane. Small-signal transmission $T_0 = 0.0946$. The curves are calculated for $\sigma_{ex,L} = 0$ (1), 3.7×10^{-17} cm^2 (2), 4.2×10^{-17} cm^2 (3), 4.7×10^{-17} cm^2 (4). (b) DPSP-PPV in 1,4-dioxane. $T_0 = 0.1045$. $\sigma_{ex,L} = 0$ (1), 4×10^{-17} cm^2 (2), 4.75×10^{-17} cm^2 (3), 5.5×10^{-17} cm^2 (4).

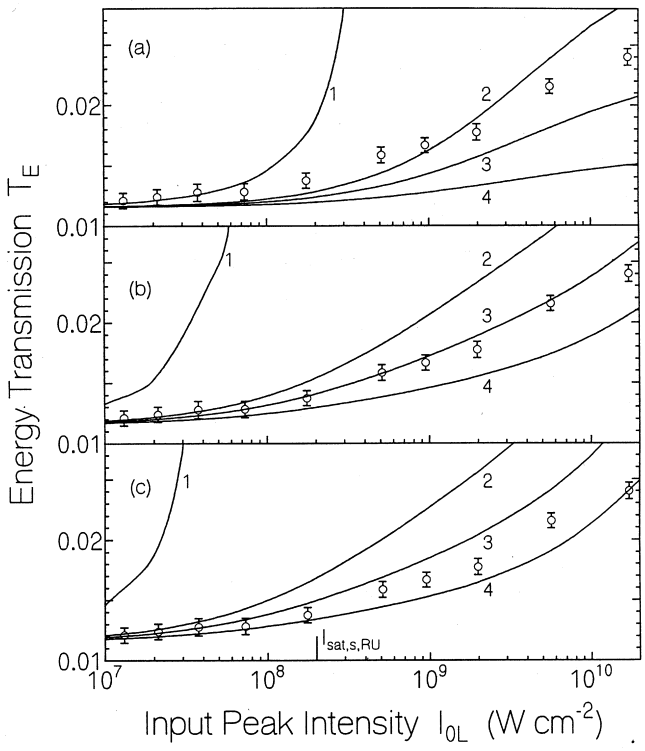

Fig. 12. Energy transmission through DPOP-PDPV in 1,4-dioxane. $T_0 = 0.0112$. $l = 1$ mm. Circles, experimental data (repeated in (a)–(c)). Curves are calculated. (a) $m_{seg} = 1$. $\sigma_{ex,L} = 0$ (1), 6×10^{-17} cm^2 (2), 6.75×10^{-17} cm^2 (3), 7.5×10^{-17} cm^2 (4). (b) $m_{seg} = 6$. $\sigma_{ex,L} = 0$ (1), 6.5×10^{-17} cm^2 (2), 7×10^{-17} cm^2 (3), 7.5×10^{-17} cm^2 (4). (c) $m_{seg} = 10$. $\sigma_{ex,L} = 0$ (1), 6.5×10^{-17} cm^2 (2), 7×10^{-17} cm^2 (3), 7.5×10^{-17} cm^2 (4).

For tetraphenylethylene in 1,4-dioxane at room temperature we measured a low fluorescence quantum yield of $\phi_F \approx 1.2 \times 10^{-3}$. The fluorescence quantum distribution is shown in Fig. 14. The excitation wavelength was $\lambda_{exc} = 365$ nm. The fluorescence spectrum has its maximum at 498 nm. The absorption–emission Stokes shift is $\delta\tilde{\nu}_{abs,em} \approx 12\,000$ cm^{-1}. It is somewhat larger than for the polymers. Excitation of tetraphenylethylene at $\lambda_{exc} = 312$ nm leads to photochemical reactions (probably formation of diphenylphenanthren) showing up in a fluorescence band peaking at 400 nm (not shown in Fig. 14).

The true radiative lifetime, τ_{rad}, of the emitting chromophore is given by $\tau_{rad} = \tau_F/\phi_F$. A comparison of the repeat-unit-based radiative lifetime, $\tau_{rad,RU}$, with the real radiative lifetime, τ_{rad}, gives access to the number of repeat units, m_e, forming an emitting chromophore. The relation is

$$m_e = \frac{\tau_{rad,RU}}{\tau_{rad}}. \quad (4)$$

The data presented in Table 1 lead to $m_e \approx 2$ for the diphenyl-substituted phenylenevinylene polymers DPOP-PPV and DPSP-PPV in 1,4-dioxane, and they lead to $m_e \approx 1$ for the diphenyl-substituted diphenylene polymers DPOP-PDPV and DFP-PDPV in 1,4-dioxane. The additional main-chain phenyl group seems to make the chain so flexible to disorder adjacent repeat units and to localize the emitting chromophore (electronic excitation extension) to one repeat unit. The emitting chromophore sizes are found to be a factor of two larger for the polymers in neat films than in in 1,4-dioxane solution. The rigid matrix seems to be responsible for the extension of the electron delocalization.

4.3. Saturable absorption analysis

The intensity-dependent energy transmission results are analysed to gain information on the segment conformational relaxation behaviour. Transmission changes are expected due to ground-state depopulation. The saturation intensity, $I_{sat,s}$, of ground-state depopulation of slow saturable absorbers (pump pulse duration, Δt_L, shorter than fluorescence lifetime, τ_F) is given by [45]

$$I_{sat,s} = \frac{h\nu_L}{\sigma_{a,L,seg}\Delta t_L} = \frac{h\nu_L}{\sigma_{a,L} m_{seg}\Delta t_L} = \frac{I_{sat,s,RU}}{m_{seg}}, \quad (5)$$

where h is the Planck constant, ν_L is the pump laser

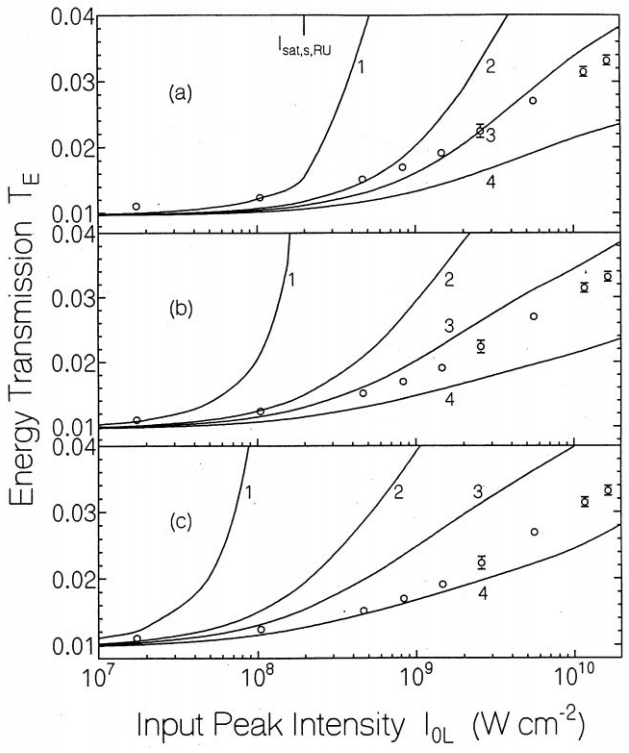

Fig. 13. Energy transmission through DFP-PDPV in 1,4-dioxane. $T_0 = 0.00956$. $l = 1$ mm. Circles, experimental data (repeated in (a)–(c)). Curves are calculated. (a) $m_{seg} = 1$. $\sigma_{ex,L} = 0$ (1), 4.2×10^{-17} cm^2 (2), 5.2×10^{-17} cm^2 (3), 6.2×10^{-17} cm^2 (4). (b) $m_{seg} = 3$. $\sigma_{ex,L} = 0$ (1), 4.67×10^{-17} cm^2 (2), 5.67×10^{-17} cm^2 (3), 6.67×10^{-17} cm^2 (4). (c) $m_{seg} = 6$. $\sigma_{ex,L} = 0$ (1), 4.67×10^{-17} cm^2 (2), 5.67×10^{-17} cm^2 (3), 6.67×10^{-17} cm^2 (4).

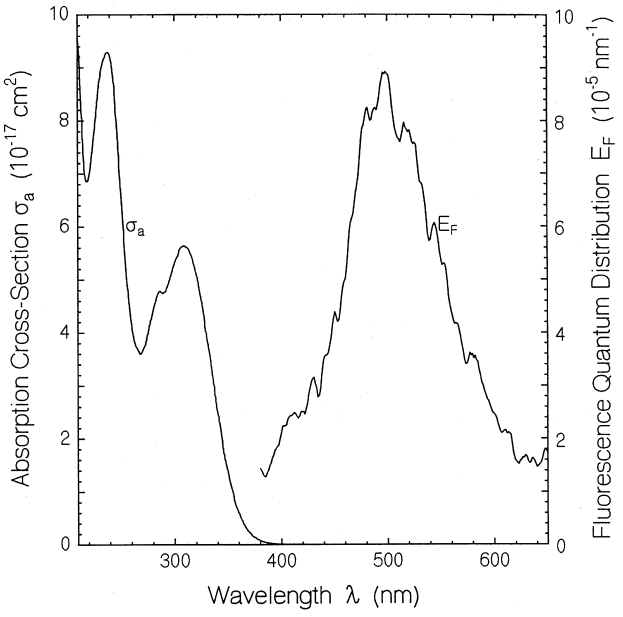

Fig. 14. Absorption cross-section spectrum, $\sigma_a(\lambda)$, and fluorescence quantum distribution, $E_F(\lambda)$, of tetraphenylethylene in 1,4-dioxane at room temperature. Excitation wavelength is $\lambda_{exc} = 365$ nm.

frequency, $\sigma_{a,L,seg} = m_{seg}\sigma_{a,L}$ is the absorption cross-section of the polymer segment which changes its absorbing position by single photon absorption, m_{seg} is the number of repeat units forming an absorption segment, $\sigma_{a,L}$ is the repeat-unit-based absorption cross-section at the laser wavelength and Δt_L is the pump pulse duration. $I_{sat,s,RU} = h\nu_L/(\sigma_{a,L}\Delta t_L)$ is the repeat-unit-based slow-absorber saturation intensity. The $I_{sat,s,RU}$ values are listed in Table 1 and are indicated in Figs. 11–13.

For the diphenyl-substituted phenylenevinylene polymers DPOP-PPV and DPSP-PPV the energy transmission practically does not change with intensity up to the highest applied values. This transmission behaviour indicates that the excited-state absorption is approximately equal to the ground-state absorption and it hinders a determination of absorption segment size, m_{seg}. The diphenyl-substituted diphenylenevinylene polymers DPOP-PDPV and DFP-PDPV show a slight rise in transmission at high intensities. This transmission dependence allows the determination of the average repeat-unit-based excited-state absorption cross-section, $\sigma_{ex,L}$, and of the absorption segment size, m_{seg}.

The polymer absorption dynamics, relevant for our analysis, is illustrated in Fig. 15a. The polymer chain is subdivided in segments (absorption segments which change their energetic position due to single-photon absorption), chromophores (regions of electronic delocalization, Frenkel-type excitons [33–35], emitting entities consisting of m_e repeat units), and repeat units. Single-photon absorption excites a chromophore from the ground-state to an excited-state (a). Excited-state conformational relaxation (b) brings the segment and the excited chromophore into new energetic positions (c) (lattice relaxation [46], relaxation time, τ_{con}). During the lifetime of the relaxed excited segment state (c) there occurs excited-state absorption (from lower occupied orbitals to segment HOMO position, from excited chromophore LUMO position to higher excited states, from higher excited states to still higher excited levels, and from relaxed segment ground-state (HOMO) to an excited state). After radiative or nonradiative relaxation of the excited chromophore back to the ground-state, there occurs ground-state conformational relaxation (d) towards the initial energetic segment position (e).

For numerical simulations the absorption model of Fig. 15a is translated to the level scheme depicted in Fig. 15b. The absorption starts from the S_0 ground-state level 1. Since a segment is removed from its initial absorption position, the ground-state absorption cross-section is $\sigma_{a,L,seg} = m_{seg}\sigma_{a,L}$ and the number density of interacting particles is $N_{seg} = N_0/m_{seg}$, where N_0 is the number density of repeat units. The various excitation processes which invoke the energetically repositioned segment are described by an average segment excited-state

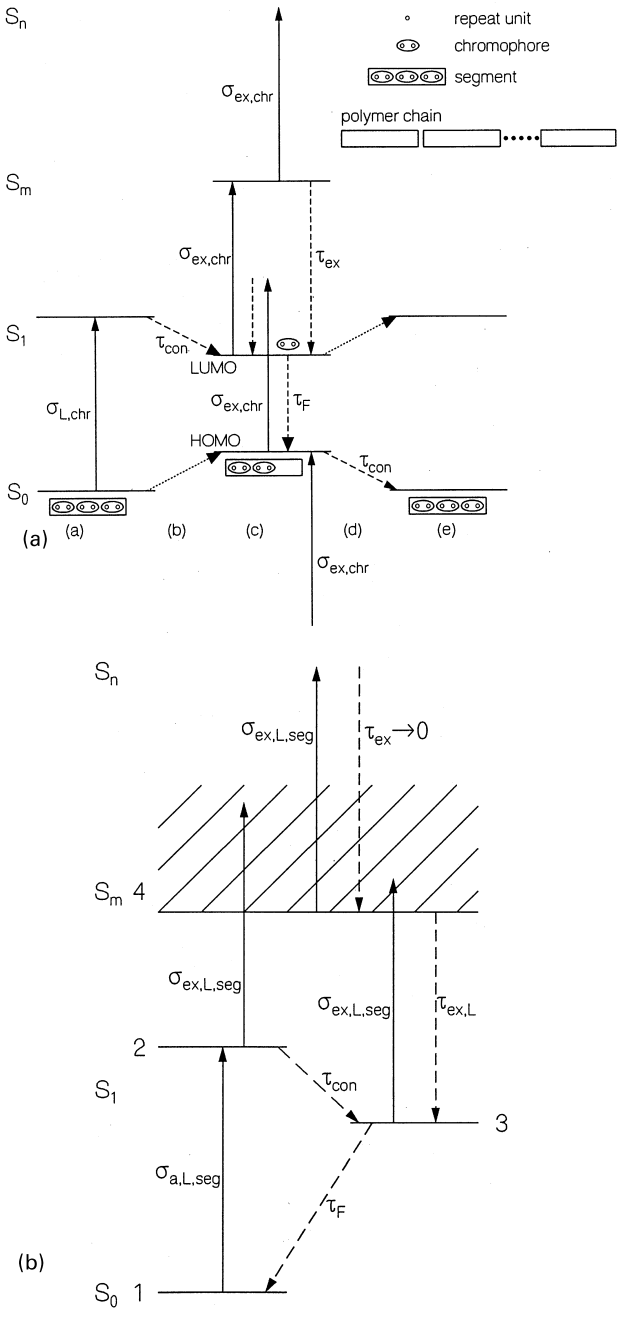

Fig. 15. (a) Energetic model for absorption dynamics. Repeat unit, chromophore, segment and polymer chain are illustrated. (a) Ground-state absorption (excitation of a chromophore in a segment, absorption cross-section $\sigma_{L,chr}$). (b) Excited-state conformational relaxation (time-constant τ_{con}). (c) Absorption processes acting on relaxed segment (average absorption cross-section $\sigma_{ex,chr}$) and radiative and nonradiative S_1–S_0 relaxation (time constant τ_F). (d) Ground-state conformational relaxation (time constant τ_{con}) to initial ground-state situation (e). (b) Energy level scheme used for numerical simulations.

absorption cross-section, $\sigma_{ex,L,seg} = m_{seg}\sigma_{ex,L}$. An open-ended system is considered, i.e. higher excited states are considered to absorb as strong as first excited states (same $\sigma_{ex,L,seg}$ and immediate back relaxation to the higher excited state).

The absorption dynamics of the level system of Fig. 15b is described by the following differential equation system [47] where $N_i(r, z', t', \theta)$ with $i = 1, 4$ denotes the level population number densities and $I_L(r, z', t')$ is the pump pulse intensity.

$$\frac{\partial N_1}{\partial t'} = -\frac{3\sigma_{a,L,seg}\cos^2(\theta)}{h\nu_L}(N_1 - N_2)I_L + \frac{N_3}{\tau_F} - \frac{N_1 - \bar{N}_1}{\tau_{or}}, \tag{6}$$

$$\frac{\partial N_2}{\partial t'} = \frac{3\sigma_{a,L,seg}\cos^2(\theta)}{h\nu_L}(N_1 - N_2)I_L - \frac{3\sigma_{ex,L,seg}\cos^2(\theta)}{h\nu_L}\left(N_2 - \frac{N_2}{N_2 + N_3}N_4\right)I_L - \frac{N_2}{\tau_{con}} - \frac{N_2 - \bar{N}_2}{\tau_{or}} \tag{7}$$

$$\frac{\partial N_3}{\partial t'} = \frac{N_2}{\tau_{con}} - \frac{3\sigma_{a,L,seg}\cos^2(\theta)}{h\nu_L}\left(N_3 - \frac{N_3}{N_2 + N_3}N_4\right)I_L + \frac{N_4}{\tau_{ex,L}} - \frac{N_3}{\tau_F} - \frac{N_3 - \bar{N}_3}{\tau_{or}} \tag{8}$$

$$\frac{\partial N_4}{\partial t'} = \frac{3\sigma_{a,L,seg}\cos^2(\theta)}{h\nu_L}(N_2 + N_3 - N_4)I_L - \frac{N_4}{\tau_{ex,L}} \tag{9}$$

$$\frac{\partial I_L}{\partial z'} = -3\sigma_{a,L,seg}I_L\int_0^{\pi/2}(N_1 - N_2)\cos^2(\theta)\sin(\theta)\,d\theta - 3\sigma_{ex,L,seg}I_L\int_0^{\pi/2}(N_2 + N_3)\cos^2(\theta)\sin(\theta)\,d\theta - \alpha^{(2)}I_L^2 \tag{10}$$

$$\bar{N}_i = \int_0^{\pi/2} N_i(\theta)\sin(\theta)\,d\theta \qquad i = 1, 2, 3, 4 \tag{11}$$

The moving-frame transformation $t' = t - nz/c_0$ and $z' = z$ is used, where t is the time, z is the propagation coordinate, n is the refractive index and c_0 is the vacuum light velocity. θ is the angle between the molecular transition dipole moment and the polarization direction of the pump laser [48]. $\bar{N}_i$ is the orientation-averaged population number density of level i. $\alpha^{(2)}$ is the two-photon absorption coefficient of the solvent ($\alpha^{(2)} = 2.6 \times 10^{-10}$ cm W^{-1} for 1,4-dioxane, the two-photon absorption cross-sections reported in Refs. [49,50] are approximately a factor of 2 too large as found by new energy density calibration).

The initial conditions are $N_1(r, t' = -\infty, z', \theta) = N_{seg} = N_0/m_{seg}$, $N_2(r, t' = -\infty, z', \theta) = N_3(r, t' = -\infty, z', \theta) = N_4(r, t' = -\infty, z', \theta) = 0$ and $I_L(r, t', z' = 0) = I_{0L}\exp(-r^2/r_L^2)\exp(-t'^2/t_L^2)$. $N_0 = CN_A$ is the total repeat unit

number density, C is the repeat unit concentration, N_A is the Avogadro constant, r is the radial coordinate and r_L and t_L are the $1/e$-intensity pump beam radius and the pump pulse duration, respectively.

The pump pulse energy transmission is

$$T_E = \frac{\int_0^\infty r\,dr \int_{-\infty}^{\infty} I_L(r,\ell,t')\,dt'}{\int_0^\infty r\,dr \int_{-\infty}^{\infty} I_L(r,0,t')\,dt'}, \quad (12)$$

where ℓ is the sample thickness.

The curves in Figs. 11–13 are calculated $T_E(I_{0L})$ dependencies using the Eqs. (6)–(12). The parameters used in the calculations are listed in Table 1 and in the figure captions. The segment size, m_{seg}, and the segment-based excited-state absorption cross-section, $\sigma_{ex,L,seg} = m_{seg}\sigma_{ex,L}$, are varied. The best-fitting values are listed in Table 1.

The diphenyl-substituted phenylenevinylene polymers DPOP-PPV and DPSP-PPV are characterized by $\sigma_{ex,L} \approx \sigma_{a,L}$. The segment size is not accessible since practically no transmission change occurs. The diphenyl-substituted diphenylenevinylene polymers give a small rise in transmission. For DPOP-PDOPV the rise in transmission from $T_E = 0.012 \pm 0.001$ at $I_{0L} = 10^7$ W cm^{-2} to $T_E = 0.0178 \pm 0.001$ at $I_{0L} = 10 \times I_{sat,s,RU} = 2 \times 10^9$ W cm^{-2} is too small to estimate a reasonably correct absorption segment size m_{seg}. Fig. 12a indicates $m_{seg} > 1$. The real value of m_{seg} may be in the range between 2 and 10. For DFP-PDPV the experimental energy transmissions and the calculated curves fit reasonably well for $m_{seg} = 3 \pm 1$ and $\sigma_{ex,L} = (6 \pm 0.3) \times 10^{-17}$ cm^2. DPOP-PDPV has the smallest degree of polymerization ($DP_w = M_w/M \approx 40$, see Fig. 1). DFP-PDPV has the largest degree of polymerization ($DP_w \approx 177$).

5. Conclusions

Two diphenyl-substituted phenylenevinylene polymers and two diphenyl-substituted diphenylenevinylene polymers in solution and as neat films have been characterized by absorption spectroscopy, fluorescence spectroscopy and saturable absorption spectroscopy. The chromophore size (electronic delocalization, emitting entity) has been derived from fluorescence quantum yield and fluorescence lifetime measurements to be two (four) for the phenylenevinylene polymers in 1,4-dioxane (neat film) and one (two) for the diphenylenevinylene polymers in 1,4-dioxane (neat film). The size of segments reacting to single-photon absorption (absorption segments) has been determined by saturable absorption studies and is found to be larger than the chromophore size.

The methods described for emitting chromophore size determination and absorption segment determination are general and may be used for chromophore size and segment size determination of other luminescent polymers.

The polymers analysed here are charge transporting and are highly luminescent in the solid state. They are therefore important layer materials for organic LEDs. In own travelling-wave lasing studies [51] the polymers studied here gave us no indication of amplified spontaneous emission.

Acknowledgements

The authors thank the Commission of the European Communities for support under ESPRIT contract 28580 "A Novel Approach to Solid State Short Wavelength Laser Generation Using Luminescent Polymers (LUPO)" which enabled this collaborative work.

References

[1] Gabler Th, Waldhäusl R, Bräuer A, Bartuch U, Stockmann R, Hörhold H-H. Opt Commun 1997;137:31.
[2] Gabler Th, Waldhäusl R, Bräuer A, Michelotti F, Hörhold H-H, Bartuch U. Appl Phys Lett 1997;70:928.
[3] Gabler T, Bräuer A, Waldhäusl R, Bartuch U, Hörhold H-H, Michelotti F. Pure Appl Opt 1998;7:159.
[4] Gabler T, Bräuer A, Hörhold H-H, Pertsch T, Stockmann R. Chem Phys 1999;245:507.
[5] Li HL, Rentsch S, Bergner H. Ultrafast processes in spectroscopy 1991, Institute of physics conference series, vol. 126. Bristol: Institute of Physics, 1992 (p. 231).
[6] Tak Y-H, Vestweber H, Bässler H, Bleyer A, Stockmann R, Hörhold H-H. Chem Phys 1996;212:471.
[7] Meyer H, Haarer D, Narmann H, Hörhold H-H. Phys Rev B 1995;52:2587.
[8] Scott JC, Malliaras GG. In: Hadziioannou G, van Hutten PV, editors. Semiconducting polymers. Chemistry, physics and engineering, Weinheim: Wiley-VCH, 2000.
[9] Samoc A, Samoc M, Luther-Davies B, Liebegott H, Stockmann R, Hörhold H-H. SPIE 1998;3474:79.
[10] Damerau T, Hennecke M, Hörhold H-H. Macromol Chem Phys 1995;196:1277.
[11] Opfermann J, Hörhold H-H. Z Phys Chem (Leipzig) 1980;261:1161.
[12] Rentsch S, Yang JP, Lenzner M, Bergner H. Makromol Chem, Macromol Symp 1990;37:17.
[13] Rentsch S, Stolberg H-P, Opfermann J, Hörhold H-H. Makromol Chem, Makromol Symp 1988;18:101.
[14] Resel R, Tertinek B, Tasch S, Davey A, Blau W, Hörhold H-H, Rost H, Leising G. Synth Met 1999;101:96.
[15] Johansson N, dos Santos DA, Feast WJ, Lögdlund M, Friend RH, Salanec WR. Synth Met 1999;101:130.
[16] Hörhold H-H, Helbig M. Makromol Chem, Macromol Symp 1987;12:229.
[17] Liebegott H. Dissertation, Universität Jena, 1999.
[18] Meysel H. Dissertation, Universität Jena, 1999.
[19] Hörhold H-H, Räthe H, Opfermann J. Acta Polym 1986;37:369.
[20] Hörhold H-H, Helbig M, Raabe D, Opfermann J, Stockmann R, Weiß D. Z Chem 1987;27:126.
[21] Penzkofer A, Drottleff E, Holzer W. Opt Commun 1998;158:221.
[22] Holzer W, Pichlmaier M, Drotleff E, Penzkofer A, Bradley DDC, Blau WJ. Opt Commun 1999;163:24.
[23] Holzer W, Pichlmaier M, Penzkofer A, Bradley DDC, Blau WJ. Chem Phys 1999;246:445.
[24] Penzkofer A, Leupacher W. J Luminesc 1987;37:61.
[25] Weidner P, Penzkofer A. Opt Quant Electron 1993;25:1.

[26] Holzer W, Penzkofer A, Gong S-H, Bradley DDC, Long X, Bleyer A. Chem Phys 1997;244:315.
[27] Penzkofer A, Holzer W, Gong S-H, Bradley DDC, Long X, Bleyer A, Blau WJ, Davey AP. In: Corcoran VJ, Goldman TA, editors. Proceedings of the International Conference on LASERS'98, Tuscon, AZ, December 7–11 1998. McLean, VA: STS Press, 1999 (p. 394).
[28] Wittmann M, Penzkofer A. Opt Quant Electron 1995;27:705.
[29] Wittmann M, Rotermund F, Weigand R, Penzkofer A. Appl Phys B 1998;66:453.
[30] Kogelink H. In: Tamic T, editor. Integrated optics, Topics in applied physics, vol. 7. Berlin: Springer, 1979 (p. 13).
[31] DMS-UV atlas of organic components. Weinheim: Chemie, 1966, 10/39.
[32] Stegemeyer H. Habilitionsschrift. Berlin: Humboldt Universität, 1967.
[33] Fidder H, Knoester J, Wiersma DA. J Chem Phys 1993;98:6564.
[34] Knoester J. J Chem Phys 1993;99:8466.
[35] Sparo FC. Nonlinear Opt 1995;12:275.
[36] Strickler SJ, Berg RA. J Chem Phys 1962;37:814.
[37] Birks JB, Dyson DJ. Proc R Soc London Ser A 1963;275:135.
[38] Holzer W, Penzkofer A, Gong S-H, Bradley DDC, Long X, Blau WJ, Davey AP. Polymer 1998;39:3651.
[39] Weast RC, editor. CRC handbook of chemistry and physics, 1st Student Ed. Boca Raton, FL: CRC Press, 1988.
[40] Peterson OG, Webb JP, McColgin WC, Eberly JH. J Appl Phys 1971;42:1917.
[41] Deshpande AV, Beidoun A, Penzkofer A, Wagenblast G. Chem Phys 1990;142:123.
[42] Parker CA. Photoluminescence of solutions. Amsterdam: Elsevier, 1968.
[43] Perrin F. Ann Phys 1929;12:238.
[44] Weidner P, Penzkofer A. Chem Phys 1995;191:303.
[45] Hercher M. Appl Opt 1967;6:947.
[46] Greenham NC, Friend RH. In: Ehrenreich H, Spaepen F, editors. Solid state physics, vol. 49. San Diego, CA: Academic Press, 1995 (p. 2).
[47] Penzkofer A, Beidoun A, Daiber M. J Luminesc 1992;51:297.
[48] Feofilov PP. The physical basis of polarized emission. New York: Consulting Bureau, 1964 (p. 108).
[49] Gong S-H, Penzkofer A. Opt Quant Electron 1999;31:269.
[50] Gong S-H, Penzkofer A. Opt Quant Electron 1999;31:1145.
[51] Holzer W, Penzkofer A, Schmitt T, Hartmann A, Bader C, Tillmann H, Raabe D, Stockmann R, Hörhold H-H. Opt Quant Electron, in press.
[52] Penzkofer A, Falkenstein W, Kaiser W. Chem Phys Lett 1976;44:82.
[53] Graf F, Penzkofer A. Opt Quant Electron 1989;17:53.